# From kesterite to stannite photovoltaics: Stability and band gaps of the $Cu_2(Zn,Fe)SnS_4$ alloy

Taizo Shibuya,[1,a)] Yosuke Goto,[2] Yoichi Kamihara,[2] Masanori Matoba,[2] Kenji Yasuoka,[1] Lee A. Burton,[3] and Aron Walsh[3,a)]
[1]*Department of Mechanical Engineering, Keio University, Yokohama 223-8522, Japan*
[2]*Department of Applied Physics and Physico-Informatics, Keio University, Yokohama 223-8522, Japan*
[3]*Centre for Sustainable Chemical Technologies, Department of Chemistry, University of Bath, Bath BA2 7AY, United Kingdom*

(Received 19 November 2013; accepted 31 December 2013; published online 15 January 2014)

Kesterite semiconductors, particularly $Cu_2ZnSnS_4$ (CZTS), have attracted attention for thin-film solar cells. We investigate the incorporation of Fe into CZTS to form the $Cu_2(Zn,Fe)SnS_4$ solid-solution for tuning the lattice spacing and band gap. First-principles calculations confirm a phase transition from kesterite (Zn-rich) to stannite (Fe-rich) at Fe/Zn $\sim$ 0.4. The exothermic enthalpy of mixing is consistent with the high solubility of Fe in the lattice. There is a linear band-gap bowing for each phase, which results in a blue-shift of photo-absorption for Fe-rich alloys due to the confinement of the conduction states. We propose compositions optimal for Si tandem cells.  [http://dx.doi.org/10.1063/1.4862030]

The first-wave of thin-film solar cell technologies resulted in the success of CdTe and $CuInSe_2$ devices. Now, there is a focus on finding alternate, earth-abundant absorber materials that could support a terawatt scale photovoltaic industry.[1] Systems of interest include $Cu_2S$,[2,3] $FeS_2$,[4,5] SnS,[6–8] and the quaternary semiconductor $Cu_2ZnSnS_4$ (CZTS).[9–12] Solar cells based on CZTS have reached 12% light-to-electricity conversion efficiency, making it the leading candidate in the field.[13–15] While CZTS itself has many attractive properties for solar cells, further increases in the performance will require optimisation that can be achieved through control of the materials stoichiometry and/or incorporation of extrinsic impurities, such as Fe (to replace Zn and form CFTS) or Se (to replace S).[16,17] In particular, Fe is of interest for Si-based tandem solar cells since the lattice constant of Si lies between two end members of the alloy, CZTS and CFTS, and an increase in the band gap could also be beneficial.

The theory of binary ($A_xB_{1-x}$) and pseudo-binary (e.g., $A_xB_{1-x}X$ or $A_xB_{1-x}XY$) semiconductor alloys is well developed.[18–20] Ordering of the binary elements can occur along fundamental crystal planes, e.g., (001), (111), and (201) orientations for the face-centred-cubic (fcc) zincblende structure, or they can be distributed in a homogeneous fashion as a disordered alloy. Quaternary semiconductors such as $Cu_2ZnSnS_4$ can be viewed as a mixture of their component binary semiconductors (i.e., $Cu_2S$, ZnS, and $SnS_2$) with specific ordering of the metals.[21] For example, the kesterite and stannite mineral structures can be described by the same $1 \times 1 \times 2$ zincblende superlattice with Cu, Zn, and Sn occupying distinct fcc lattice sites (Fig. 1).

Kesterite and stannite are structurally similar but distinct mineral structures: the former is known for $Cu_2ZnSnS_4$ and the latter for $Cu_2FeSnS_4$;[22] although, the energy difference between the two polymorphs is small. For the $Cu_2(Zn,Fe)SnS_4$ solid solution, the structural transition from kesterite to stannite is suggested as the Zn:Fe ratio decreases.[23,24] Unfortunately, due to their structural similarity, the complete determination of the transition is challenging. It should also be noted that standard X-ray diffraction can not distinguish between Cu and Zn due to their similar cross-sections; a synchrotron light or neutron source is required for that purpose[25] as well as for determining secondary phases.[26] For the Fe/Zn system, a neutron diffraction study which reports complex cation disorder is available.[24]

In this Letter, we combine a quantum mechanical description of the total energy and electronic structure with a statistical mechanical description of the solid-solution to predict the structural and electronic properties of the Fe/Zn alloy from first-principles. The predictive value of atomistic modelling for this class of materials has been well established,[11] and our results provide guidelines for expanding their range of applications.

The $Cu_2Zn_{1-x}Fe_xSnS_4$ alloy was modeled using a $2 \times 2 \times 1$ supercell of the conventional tetragonal kesterite/stannite crystal structures. In this 64-atom supercell, Zn/Fe atoms occupy 8 distinct lattice sites. We have calculated $x = 0$, 0.25, 0.5, 0.75, and 1 for kesterite and stannite, which correspond to 2, 4, and 6 Zn substitutions by Fe. To describe

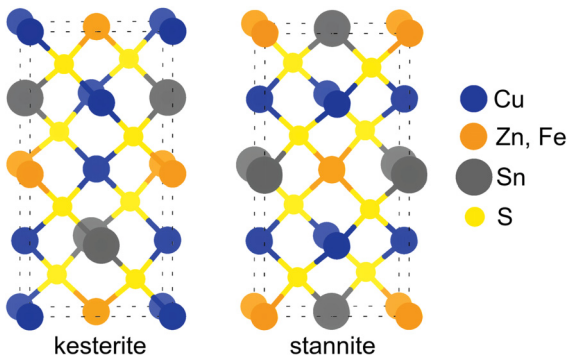


FIG. 1. Illustration of the conventional tetragonal unit cells of kesterite (space group $I\bar{4}$) and stannite (space group $I\bar{4}2m$).

a)Electronic addresses: tzo@z6.keio.jp and a.walsh@bath.ac.uk

 

the site occupation, we considered all symmetry inequivalent configurations using the Site Occupation Disorder[27] approach. These were used to construct a statistical representation of the disordered alloy at an equilibrium temperature $T$, assuming a representative annealing temperature of 750 °C. For $x = 0.25$ and 0.75 there are ${}_8C_2 = 28$ (3 unique) configurations and $x = 0.5$ there are ${}_8C_4 = 70$ (6 unique) configurations.

The total energy and band structures were obtained using density functional theory within the generalized gradient approximation (PBE),[28] as implemented in the plane-wave code VASP.[29,30] The core-valence interaction was treated within the projector-augmented wave scheme.[31] In order to overcome semi-local description of electron exchange and correlation, we employed screened hybrid functional of Heyd, Scuseria, and Ernzerhof (HSE06)[32] The HSE screening parameter was set to 0.2 $Å^{-1}$. A plane-wave cutoff of 400 eV was used, and the Brillouin-zone sampled at the zone-centre with $\sigma = 0.05$ eV (density of states were calculated using a $2 \times 2 \times 2$ $k$-mesh).

The linear band-gap bowing coefficients ($b$) were obtained from the relation

$$E_g(x) = (1-x)E_g^{Cu_2ZnSnS_4} + (x)E_g^{Cu_2FeSnS_4} - bx(1-x), \quad (1)$$

where $E_g$ is the calculated band gap of the alloy at composition $x$. The mixing enthalpy ($\Delta H$) with respect to the parent quaternary compounds was calculated from the total energies ($E$)

$$\Delta H(x) = E(x) - [(1-x)E_{Cu_2ZnSnS_4} + (x)E_{Cu_2FeSnS_4}]. \quad (2)$$

The lattice constants and band gaps ($E_g^\Gamma$) of CZTS and CFTS, in both the kesterite and stannite structures, are summarized in Table I. First, we discuss the experimentally observed structures, kesterite CZTS (ke-CZTS) and stannite CFTS (st-CFTS). The lattice parameters for ke-CZTS are $a = 5.454$ Å and $c = 10.885$ Å, which are within 1% of the experimentally reported values.[24] The calculated band gap of 1.54 eV is close to the reported 1.44–1.51 eV.[33–35]

The lattice constants of st-CFTS are $a = 5.489$ Å and $c = 10.760$ Å, which are also within 1% of the experimentally reported values.[24] We calculated the band gap of st-CFTS to be 1.8 eV; note, this is a quasiparticle gap, which excludes on-site excitations associated with the Fe $d$ band. For st-CFTS, there is no experimental consensus on a band gap value, but in nanocrystalline form it varies from 1.25 to 1.5 eV.[36–38] In contrast, the empirical relation proposed for multicomponent semiconductors by Matsushita *et al.*,[39] predicts a value of 1.6 eV, which is larger than ke-CZTS.

With regards to the less-stable polymorphs, st-CZTS has $a = 5.431$ Å and $c = 10.956$ Å. Compared to ke-CZTS, $a$ is reduced and $c$ is expanded. This behaviour can be understood by the ionic view of $Cu^+$, $Zn^{2+}$, $Sn^{4+}$, and $S^{2-}$, which explains the energetics of CZTS on electrostatic grounds.[40,41] The equilibrium parameters for ke-CFTS are $a = 5.426$ Å and $c = 11.038$ Å. The $a$-axis shrinks and $c$-axis expands compared to st-CFTS. The band gaps of st-CZTS and ke-CFTS are 1.36 eV and 1.70 eV, respectively, which are both smaller than the more stable polymorphs in agreement with previous reports.[40,41]

For $x = 1$, the Zn site is fully occupied by Fe, which makes this material magnetic. The Fe(II) oxidation state ($d^6$) in a tetrahedral environment results in a local magnetic moment of approximately 4 $\mu_B$, i.e., $e_d^3 t_{2d}^3$. These spins can order in-phase (ferromagnetic, FM) or out-of-phase (antiferromagnetic, AFM). Stannite structured CFTS has a Néel temperature as low as 6–8 K;[42,43] however, its microscopic magnetic structure is not clear. To check the magnetic ordering and its stability, we calculated three magnetic structures for ke-CFTS and st-CFTS. The results are summarized in Table II. As shown in Fig. 1, kesterite and stannite contain Cu-Fe and Sn-Fe (001) layers, respectively. In addition to the FM configuration, we considered two antiferromagnetic configurations on those layers, denoted as stripe-AFM and checkerboard-AFM, respectively. In stripe-AFM, the magnetic moments of Fe align in rows, whereas in checkerboard-AFM the neighboring Fe atoms always have opposite moments.

TABLE I. Calculated and experimental[24] structural and electronic properties of kesterite and stannite $Cu_2ZnSnS_4$ ($x = 0.0$) and corresponding $Cu_2FeSnS_4$ ($x = 1.0$), denoted as ke-CZTS, st-CZTS, ke-CFTS, and st-CFTS, respectively.

| | $a$(Å) | | $c$(Å) | | |
|---|---|---|---|---|---|
| Structure | Calculated | Experimental | Calculated | Experimental | $E_g^\Gamma$ (eV) |
| ke-CZTS | 5.454 | 5.428 | 10.885 | 10.864 | 1.54 |
| st-CZTS | 5.431 | | 10.956 | | 1.36 |
| ke-CFTS | 5.426 | | 11.038 | | 1.74 |
| st-CFTS | 5.489 | 5.444 | 10.760 | 10.729 | 1.85 |

TABLE II. Properties for three magnetic structures of CFTS and their stability in the kesterite and stannite structures, denoted as ke-CFTS and st-CFTS, including lattice constants and band gap. Ferromagnetic order, stripe-type antiferromagnetic order, and checkerboard antiferromagnetic order in Fe are denoted by FM, stripe-AFM, and checkerboard-AFM, respectively. The band gap of both spin-up and spin-down channel are shown together with their average. $\Delta E$ is the relative total energy referenced to the FM configuration.

| | | | | | $E_g^\Gamma$[eV] | | |
|---|---|---|---|---|---|---|---|
| Structure | Fe-order | $\Delta E$ (meV/atom) | $a$ (Å) | $c$ (Å) | Spin-up | Spin-down | Average |
| ke-CFTS | FM | 0 | 5.426 | 11.038 | 1.54 | 1.95 | 1.74 |
| | Stripe-AFM | −12.0 | 5.424 | 11.036 | 1.73 | 1.73 | 1.73 |
| | Checkerboard−AFM | −18.5 | 5.426 | 11.038 | 1.70 | 1.70 | 1.70 |
| st-CFTS | FM | 0 | 5.489 | 10.760 | 1.52 | 2.18 | 1.85 |
| | Stripe-AFM | −14.2 | 5.488 | 10.758 | 1.84 | 1.84 | 1.84 |
| | Checkerboard-AFM | −6.5 | 5.489 | 10.757 | 1.79 | 1.79 | 1.79 |

For all of the magnetic configurations considered, the calculated local magnetic moment of Fe is about 3.5 $\mu_B$, confirming the high-spin state. As expected, antiferromagnetic ordering is lowest in energy for st-CFTS; however, we found stripe-AFM and checkerboard-AFM to be stable for stannite and kesterite, respectively. The energy difference between alternative configurations is small, consistent with the low Néel temperature. The magnetic configuration shows no strong influence on the crystal structure or electronic properties. Indeed, the average band gap of spin-up and spin-down for the FM configurations gives almost the same value as the AFM states. For the alloy, we therefore assume a FM structure and compute the band gap averaged over both spin channels.

The energy difference between the kesterite and stannite polymorphs for the alloy is shown in Fig. 2. The stannite structure becomes more stable than kesterite in the range of $x > 0.4$. The associated evolution of the tetragonal distortion parameter is plotted in Fig. 3. As expected, at $x = 0$ and 0.25 the kesterite values match the experimental data, while at $x = 0.50$, 0.75, and 1, the values of stannite fall on the experimental curve. From this agreement, as well as the fact that the lattice parameters of the end members match experiment, we conclude that phase transition occurs at about $x = 0.4$. While, partial cation-disorder hinders the observation of a clear transition point,[23,24] recent Raman scattering measurements support our prediction.[44]

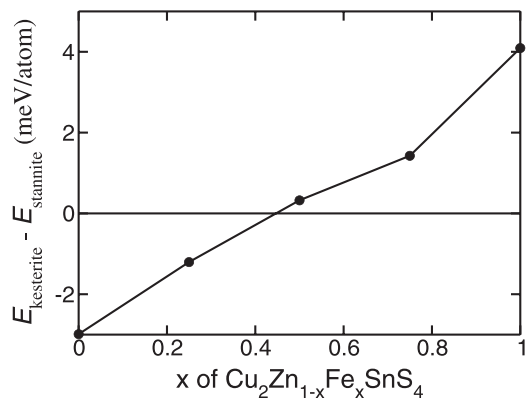


FIG. 2. Total energy difference between kesterite and stannite with respect to Fe composition $x$. Where negative, kesterite is stable; where positive, stannite is stable.

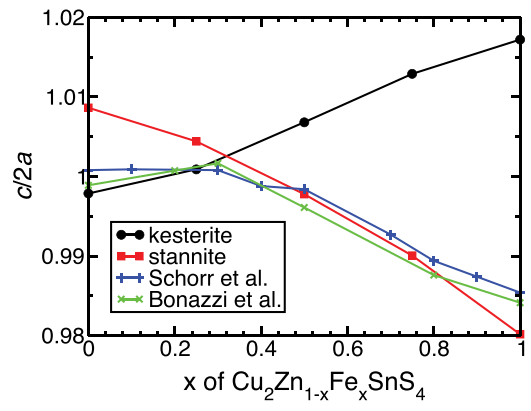


FIG. 3. Calculated and experimental[23,24] $c/2$ $a$ with respect to Fe composition $x$.

The predicted mixing enthalpy is negative (exothermic) for both kesterite and stannite (Fig. 4), implying that alloy formation is a thermodynamically favourable process. Similar behaviour is seen in I-III-V semiconductor alloys.[45] The stable mixing is consistent with the fact that the natural minerals of kesterite and stannite occur in alloy form,[22] where the equilibrium Fe composition frequently exceeds 25%. At $x = 0.50$ and 0.75, kesterite has lower mixing enthalpy than stannite, which manifests as a slight deviation from linear behavior in that region (Fig. 2).

The band gap dependence on composition is illustrated in Fig. 5. Both kesterite and stannite have small quadratic bowing coefficients, suggesting that the alloy is "well-behaved" in both phases. The band gap increases as the Fe ratio increases: contributions of Zn $s$ orbitals to the delocalised conduction band are replaced by the more localised Fe $d$ orbitals, which results both in a decrease in band width and a spatial confinement of the electronic wavefunction. While linear behaviour is observed for the kesterite and stannite structures, separately, there will be a transition between them at ca. $x = 0.4$, which may result in a small discontinuity experimentally. The flat region could be useful to search for quaternary materials with optimal photovoltaic band gaps, where previously Si and Ge replacements have been of interest.[33,46,47]

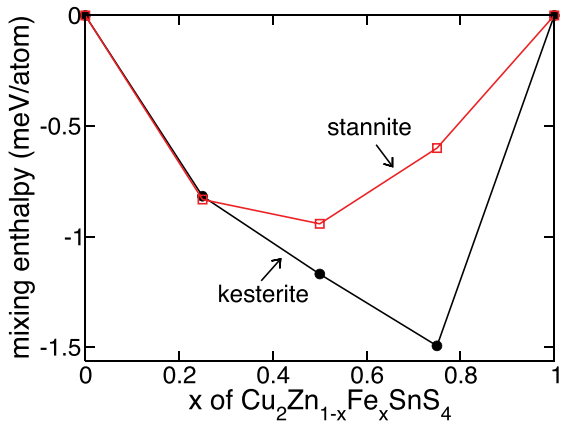


FIG. 4. Mixing enthalpy of kesterite and stannite at different Fe compositions ($x$).

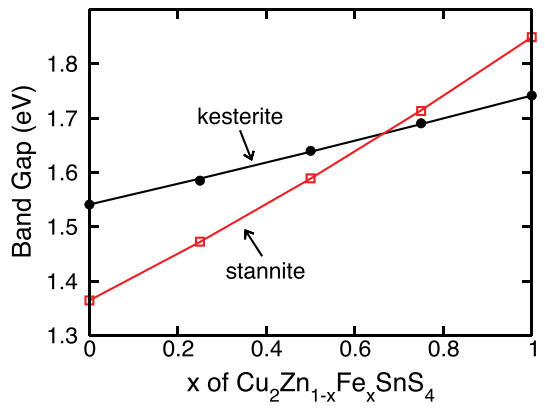


FIG. 5. Calculated band gap of kesterite and stannite as a function of Fe composition. The linear band-gap bowing coefficients $b$ of kesterite and stannite are 0.01 eV and 0.07 eV, respectively. The definition of $b$ is found in Eq. (1) in text.

It has been suggested that organic or dye-sensitised absorbers could make an inexpensive top layer on Si to form a more efficient tandem cell.[48] Moving to two-junction photovoltaics increases the limiting efficiency considerably. The ease of incorporation of Fe in CZTS allows for the selective tuning of the band gap and the lattice parameters. For Si, which has an indirect band gap of 1.12 eV at 300 K, the optimal band gap for a top layer is between 1.70 and 1.76 eV,[49] giving a theoretical efficiency of 37%.[50] The Fe/Zn alloy enters the optimal band gap region around $x = 0.8$, where stannite is thermodynamically stable (Figure 2). The predicted lattice mismatch at this composition is less than 1%, thus the fabrication of a robust heterostructure should be possible.

In conclusion, we have confirmed the high solubility of Fe in $Cu_2ZnSnS_4$ through first-principles calculations. The phase transition from kesterite to stannite is found to occur around $x = 0.4$. Despite the negative enthalpy of mixing, both the lattice constant and band gap dependence on the Fe/Zn ratio in the lattice are well behaved. The increase in band gap, and mild lattice volume decrease, for larger Fe concentrations make the alloy of interest for applications in Si-based tandem solar cells.

We acknowledge support from Grant-in-Aid for Scientific Research (Grant No. 20246040) and a Grant-in-Aid for the Global Center of Excellent Program for Center for Education and Research of Symbiotic, Safe and Secure System Design from the Ministry of Education, Culture, Sports, Science, and Technology of Japan. A.W. and L.B. benefited from membership of the UK's HPC Materials Chemistry Consortium, which is funded by EPSRC Grant No. EP/F067496.

[1]L. M. Peter, Philos. Trans. R. Soc. A **369**, 1840 (2011).
[2]K. Böer, Phys. Status Solidi A **40**, 355 (1977).
[3]S. C. Riha, S. Jin, S. V. Baryshev, E. Thimsen, G. P. Wiederrecht, and A. B. Martinson, ACS Appl. Mater. Interface **5**, 10302 (2013).
[4]S. Nakamura and A. Yamamoto, Sol. Energy Mater. Sol. Cells **65**, 79 (2001).
[5]J. Puthussery, S. Seefeld, N. Berry, M. Gibbs, and M. Law, J. Am. Chem. Soc. **133**, 716 (2011).
[6]P. Sinsermsuksakul, J. Heo, W. Noh, A. S. Hock, and R. G. Gordon, Adv. Energy Mater. **1**, 1116 (2011).
[7]L. A. Burton and A. Walsh, J. Phys. Chem. C **116**, 24262 (2012).
[8]L. A. Burton and A. Walsh, Appl. Phys. Lett. **102**, 132111 (2013).
[9]J. J. Scragg, P. J. Dale, and L. M. Peter, Electrochem. Commun. **10**, 639 (2008).
[10]K. Wang, O. Gunawan, T. Todorov, B. Shin, S. Chey, N. Bojarczuk, D. Mitzi, and S. Guha, Appl. Phys. Lett. **97**, 143508 (2010).
[11]A. Walsh, S. Chen, S.-H. Wei, and X.-G. Gong, Adv. Energy Mater. **2**, 400 (2012).
[12]T. Gershon, B. Shin, T. Gokmen, S. Lu, N. Bojarczuk, and S. Guha, Appl. Phys. Lett. **103**, 193903 (2013).
[13]T. K. Todorov, J. Tang, S. Bag, O. Gunawan, T. Gokmen, Y. Zhu, and D. B. Mitzi, Adv. Energy Mater. **3**, 34 (2013).
[14]D. A. R. Barkhouse, O. Gunawan, T. Gokmen, T. K. Todorov, and D. B. Mitzi, Prog. Photovolt. Res. Appl. **20**, 6 (2012).
[15]M. T. Winkler, W. Wang, O. Gunawan, H. J. Hovel, T. K. Todorov, and D. B. Mitzi, Energy Environ. Sci. (in press).
[16]R. Haight, A. Barkhouse, O. Gunawan, B. Shin, M. Copel, M. Hopstaken, and D. B. Mitzi, Appl. Phys. Lett. **98**, 253502 (2011).
[17]S. Chen, A. Walsh, J.-H. Yang, X. G. Gong, L. Sun, P.-X. Yang, J.-H. Chu, and S.-H. Wei, Phys. Rev. B **83**, 125201 (2011).
[18]B. Pamplin, J. Phys. Chem. Solids **25**, 675 (1964).
[19]C. Goodman, J. Phys. Chem. Solids **6**, 305 (1958).
[20]D. O. Scanlon and A. Walsh, Appl. Phys. Lett. **100**, 251911 (2012).
[21]S. Chen, X. Gong, A. Walsh, and S.-H. Wei, Phys. Rev. B **79**, 165211 (2009).
[22]S. R. Hall, J. T. Szymanski, and J. M. Stewart, Can. Miner. **16**, 131 (1978).
[23]P. Bonazzi, L. Bindi, G. P. Bernandini, and S. Menchetti, Can. Miner. **41**, 639 (2003).
[24]S. Schorr, H.-J. Hoebler, and M. Tovar, Eur. J. Miner. **19**, 65 (2007).
[25]T. Washio, H. Nozaki, T. Fukano, T. Motohiro, K. Jimbo, and H. Katagiri, J. Appl. Phys. **110**, 074511 (2011).
[26]H. Nozaki, T. Fukano, S. Ohta, Y. Seno, H. Katagiri, and K. Jimbo, J. Alloys Compd. **524**, 22 (2012).
[27]R. Grau-Crespo, S. Hamad, C. R. A. Catlow, and N. H. D. Leeuw, J. Phys.: Condens. Matter **19**, 256201 (2007).
[28]J. Perdew, K. Burke, and M. Ernzerhof, Phys. Rev. Lett. **77**, 3865 (1996).
[29]G. Kresse and J. Furthmüller, Phys. Rev. B **54**, 11169 (1996).
[30]G. Kresse and J. Furthmiiller, Comput. Mater. Sci. **6**, 15 (1996).
[31]P. E. Blöchl, Phys. Rev. B **50**, 17953 (1994).
[32]J. Heyd, G. E. Scuseria, and M. Ernzerhof, J. Chem. Phys. **118**, 8207 (2003).
[33]H. Matsushita, T. Maeda, A. Katsui, and T. Takizawa, J. Cryst. Growth **208**, 416 (2000).
[34]J.-S. Seol, S.-Y. Lee, J.-C. Lee, H.-D. Nam, and K.-H. Kim, Sol. Energy Mater. Sol. Cells **75**, 155 (2003).
[35]J. J. Scragg, P. J. Dale, and L. M. Peter, Electrochem. Commun. **10**, 639 (2008).
[36]X. Zhang, N. Bao, K. Ramasamy, Y.-H. A. Wang, Y. Wang, B. Lin, and A. Gupta, Chem. Commun. **48**, 4956 (2012).
[37]L. Li, X. Liu, J. Huang, M. Cao, S. Chen, Y. Shen, and L. Wang, Mater. Chem. Phys. **133**, 688 (2012).
[38]C. Huang, Y. Chan, F. Liu, D. Tang, J. Yang, Y. Lai, J. Li, and Y. Liu, J. Mater. Chem. A **1**, 5402 (2013).
[39]H. Matsushita, T. Ichikawa, and A. Katsui, J. Mater. Sci. **40**, 2003 (2005).
[40]J. Paier, R. Asahi, A. Nagoya, and G. Kresse, Phys. Rev. B **79**, 115126 (2009).
[41]A. Shavel, J. Arbiol, and A. Cabot, J. Am. Chem. Soc. **132**, 4514 (2010).
[42]G. P. Bernardini, D. Borrini, A. Caneschi, F. D. Benedetto, D. Gatteschi, S. Ristori, and M. Romanelli, Phys. Chem. Miner. **27**, 453 (2000).
[43]A. Caneschi, C. Cipriani, F. D. Benedetto, and R. Sessoli, Phys. Chem. Miner. **31**, 190 (2004).
[44]X. Fontané, V. Izquierdo-Roca, E. Saucedo, S. Schorr, V. Yukhymchuk, M. Y. Valakh, A. Pérez-Rodríguez, and J. Morante, J. Alloys Compd. **539**, 190 (2012).
[45]A. Walsh and S.-H. Wei, Phys. Rev. B **76**, 195208 (2007).
[46]J. J. Scragg, P. J. Dale, L. M. Peter, G. Zoppi, and I. Forbes, Phys. Status Solidi B **245**, 1772 (2008).
[47]D. M. Schleich and A. Wold, Mater. Res. Bull. **12**, 111 (1977).
[48]Z. M. Beiley and M. D. McGehee, Energy Environ. Sci. **5**, 9173 (2012).
[49]S. R. Kurtz, P. Faine, and J. M. Olson, J. Appl. Phys. **68**, 1890 (1990).
[50]C. H. Henry, J. Appl. Phys. **51**, 4494 (1980).